Polypropylene/Poly(vinyl alcohol) Blends Compatibilized with Kaolinite Janus Hybrid Particles and Their Transformation into Fibers

Xiang Yan, Aurelie Cayla, Eric Devaux, Belkacem Otazaghine, Fabien Salaun

Polypropylene/Poly(vinyl alcohol) Blends Compatibilized with Kaolinite Janus Hybrid Particles and Their Transformation into Fibers

Xiang Yan,*,† Aurélie Cayla,† Eric Devaux,† Belkacem Otazaghine,‡ and Fabien Salaün†

†GEMTEX − Laboratoire de Génie et Matériaux Textiles, ENSAIT, F-59000 Lille, France

‡Centre des Matériaux des mines d'Alès (C2MA), IMT, Mines Alès, 6, Avenue de Clavières, F-30319 Alès Cedex, France

ABSTRACT: This study focuses on the adoption of hybrid Janus kaolinite particles into immiscible PP−PVA blends for melt spinning, as an extension for the textile field. The anisotropic grafting of kaolinite by octadecylphosphonic acid allowed the localization of the particles at the PP−PVA interface. Then surface-modified PP porous fibers have been obtained by selective extraction of the PVA phase. The SEM observations and selective extraction experiments indicated that the unmodified kaolinite particles were localized within the PVA phase having limited impact on the PVA accessibility, while Janus-modified particles were distributed at the biphasic interface decreasing significantly the PVA accessibility. The volume average diameter of PVA within annealed blends is dramatically decreased from 73.3 to 13.6 μm by the addition of 5 wt % of Janus kaolinite particles, proving the strong compatibility effect. Gel-like behavior was also observed in rheological investigations for blends filled with modified kaolinite. The melt flow index (MFI) was tested for adapting the conditions of melt spinning. The PVA accessibility can reach more than 90%, and the interface-located fillers can enhance the Young's modulus of the biphasic fibers with 57% increment. The crystallization structure of the porous PP fibers was also influenced by the Janus kaolinite particles, with the enhancement of crystal perfection.

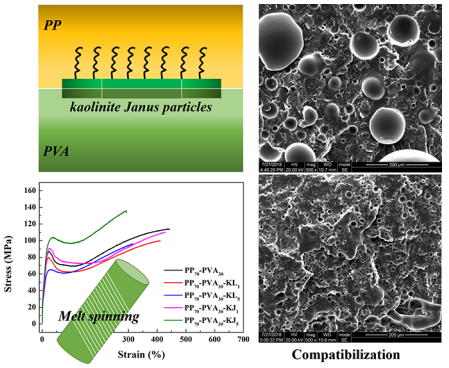

1. INTRODUCTION

Blending polymers is a common method to endow the materials with synergetic properties.[1,2] Nevertheless, most of the polymers show inherent immiscibility due to low mixing entropy,[3] resulting in heterogeneous morphology and deterioration of mechanical properties, caused by the interface as stress concentration point.[4] A surfactant is usually added to enhance the compatibilization of two phases. Block copolymers (BCPs) are one of the most conventional surfactants used. It works as a coupling agent between the two polymers forming a lot of effective joints.[5] However, it is easy to be detached from the interface under fierce shearing conditions. In addition, beyond the critical concentration, BCPs will saturate the interface, aggregate, and finally generate micelles into the bulk phases.[6]

Recently, there has been an extensive investigation about nanoparticles for compatibilization of polymer blends. A lot of candidates with different shapes and dimensions were tested, such as spherical (silica nanoparticles,[7] carbon black,[8] and gold nanoparticles[9]), cage-like (POSS[10]), patchy (clay[11] and graphene[12]), and one-dimensional (carbon nanotube (CNT)[13]) particles. The rigid core which is formed by particles at the polymer blend interface provides the Pickering effect, with the morphology stability against shearing and annealing conditions.[14] Apart from the role of compatibilization, the intrinsic functionality can also be combined with the biphasic material, such as electrical,[15] thermal conductivity,[16] and antibacterial properties.[17] However, it is often difficult for these particles to localize them at the interface. The localization of nanoparticles is tunable via tailoring their wettability when the thermodynamical factor plays the dominant role. Based on Young's model,[18] it can be concluded that the particles can only be distributed at the interface when the absolute value of the difference between the two interfacial tensions for the particle with bulk polymers is lower than that between the two phases. The harsh requirement needs a precise surface grafting for the nanoparticles often based on trial-and-error methods, and the specific surface-tailored particles are only suitable in particular biphasic systems.

To overcome the obstacle, Janus nanoparticles (JNPs) appear as a solution combining the advantages of nanoparticles (Pickering effect) and BCPs (amphiphilicity), with two different surface compositions. JNPs can strongly adsorb and orient at the biphasic polymer interface. According to the molecular simulations, it has been proved that the Janus particles exhibit a higher surface activity, compared with other homogeneously modified surfactants.[19] JNPs still work efficiently under high shear conditions.[20] Nowadays, there are bursting numbers of reports concerning the utilization of

Janus particles into polymer blends.[4,20−25] The difficulty lies in the breakage of the symmetry of the particles, for which the industrialization is hard to be realized. One of the methods is to break the symmetry of the particle skeleton. Parpaite et al.[24] synthesized a snowman-like Janus particle, combined with PS and SiO_2, for compatibilization of polystyrene (PS)-polyamide-6 (PA6) blend. Xu et al.[25] also utilized similar snowman-like particles with asymmetrical grafted chains for compatibilization of liquid isoprene rubber-epoxy resin. Nie et al.[26] grafted synthetic silica nanosheet with PS and polyisoprene (PI) chains in order to compatibilize PS−PI blend. As a matter of fact, some natural fillers show an inherent chemical composition asymmetry which leaves the possibility to modify regioselectively their surface. Most attention has been paid to the high-aspect-ratio clay derivatives, such as halloysite nanotubes (HNTs) and kaolinite. A halloysite nanotube owns silanol groups at the outer surface and aluminol groups at the inner surface. Sahnoune et al.[27] used PS regioselective functionalized halloysite for compatibilizing a PS−PA11 blend. Kaolinite is one kind of phyllosilicate (layered aluminosilicate) with the molecular formula of $Al_2Si_2O_5(OH)_4$. It possesses dioctahedral 1:1 layered silicate (polar lamellae) stacked and held together via hydrogen bonds. One tetrahedral layer of silica (SiO_4, TS layer) is linked through common apical oxygen atoms to one octahedral layer ($AlO_2(OH)_4$, OS layer).[28] Weiss et al.[29] modified kaolinite with polymer chains to obtain hybrid Janus particles. The regioselective modifications were based for one side on simple cation exchange and for the other side on covalent grafting via catechol groups. The obtained Janus kaolinite particles grafted with PS and PMMA chains were used for the compatibilization of PS−PMMA blend in a solvent casting procedure. However, the modification of both sides of kaolinite seems complicated and costly, which is not beneficial for industrial production. Is it feasible to modify one single side to obtain Janus particles with significant hybrid properties? So far, there are not any reports about the use of single side modified kaolinite for compatibilizing immiscible polymer blends.

For textile industries, the melt spinning provides an availability of fabricating fibers from biphasic polymers.[30,31] The related technology (e.g., twisting, knitting, weaving) can be applied with melt-spun fibers, playing an essential role in all corners of the industry. To best of our knowledge, there is no study on the application of Janus particles in melt spinning until now. Herein, we make efforts to extend the application of Janus particles into textile areas. The fillers at the interface can not only tune the biphasic morphology but also provide a protocol for fabricating surface-modified material. Moreover, if one of the phases can be drastically removed, surface-modified porous scaffold embedded with particles can be obtained. A lot of water-soluble polymers are good candidates for the sacrificial phase, such as poly(vinyl alcohol) (PVA),[32] polyvinylpyrrolidone (PVP),[33] sulfopolyester (SP),[34] and poly(ethylene oxide) (PEO).[17,7] The sacrificial polymer can even be reused for the repetitive production.[33] There were few reports[35] concerning the morphological control of PP−PVA blends by adding nanofillers. Therefore, our research group has made efforts to control the localization of isotropic silica nanoparticles within PP−PVA[32] and manufactured the materials into fibers by melt spinning. It has been found that 70:30 wt % is an ideal ratio for manufacturing the fibers, with a good spinnability, a high fraction of PVA removal, as well as satisfactory mechanical performance.

In this study, to improve compatibility with PP, kaolinite has been modified to make a single side (the octahedral layer) of the particles hydrophobic via regioselective grafting of octadecyl ($C_{18}H_{37}$-) groups by using octadecylphosphonic acid (ODPA), which forms a stable bulk (aluminoalkyl)-phosphonate.[36] The obtained Janus kaolinite particles were then first used in PP−PVA biphasic systems. The ternary blends were compounded by melt extrusion, and the localization of the fillers was observed by SEM. The rheological performance and the morphology of the blends were investigated. Afterward, the materials were manufactured into multifilament yarns by melt spinning technology. The evolution of PVA accessibility from extrudates to multifilaments was observed, as a clear indication of the biphasic morphology and extraction efficiency. The mechanical properties and aggregation structures of the obtained fibers were also considered.

2. EXPERIMENTAL SECTION

2.1. Materials. Polypropylene (PP; PPH 9069) was a commercial product from Total S.A. (Courbevoie, France, spinning grade), with the melting temperature of 168 °C, with melt flow index (MFI) of 15 g/10 min (200 °C, 2.16 kg). PVA (OKS-8042P) was purchased from Nichigo Gohsei (Osaka, Japan, spinning grade), with the melting point of 178 °C, with MFI of 23 g/10 min (200 °C, 2.16 kg).

Octadecylphosphonic acid (ODPA) was supplied by Specific Polymers (Montpellier, France). Ethanol and acetone were purchased from Fisher Chemical. Kaolinite (PARALUX) with a specific surface area (BET) of 12.2 ± 1.5 $m^2\ g^{-1}$, an aspect ratio α of 10, and an average primary particle size (d_{el}) of 0.8 μm was kindly supplied by Imerys (Paris, France) and denoted as KL. Surface treatment was carried out as follows: 100 g of kaolinites, 2.5 g of ODPA, and 300 mL of an ethanol/water mixture (96/4) were introduced in a 500 mL flask fitted with a condenser. The mixture was then stirred and heated at solvent reflux for 15 h. The mixture was then centrifuged to remove the liquid phase and washed three times with acetone. Finally, the modified clay was dried under vacuum before characterization. Surface treated kaolinite is referred as KJ.

All of the raw materials were used as received.

2.2. Sample Preparation. *2.2.1. PP−PVA−Kaolinite Ternary Nanocomposites.* All of the polymer blends were melt-mixed using a corotating intermeshing twin-screw extruder (Thermo Haake, a screw diameter of 16 mm, L/D = 25). The mass ratio of PP and PVA was fixed at 70/30 (wt %/wt %), whereas the weight fraction of particles (KL and KJ) was varied at two different fractions: 1 and 5 wt % in total. PP and PVA were dried in the oven at 80 °C overnight to eliminate the residual moisture inside the polymers. The temperature profiles were 160/170/180/190/200 °C in the five heating zones, with the screw rotational speed of 100 rpm. The continuously produced extrudates in the form of rods were transported by a conveyor equipped with the cooling air stream. Afterward, the cooled polymer rods were pelletized, ready for the further melt spinning. For the ternary blends, the melt extrusion procedures were segregated into two steps. First, the kaolinite nanoparticles were precompounded with PP; second, the prepared blends were extruded again with PVA to obtain the PP−PVA−kaolinite ternary blends.

The samples containing unmodified kaolinite (KL) and modified kaolinite (KJ) are denoted as PP_{70}-PVA_{30}-KL_x and PP_{70}-PVA_{30}-KJ_x, respectively. x represents the wt % of filler in

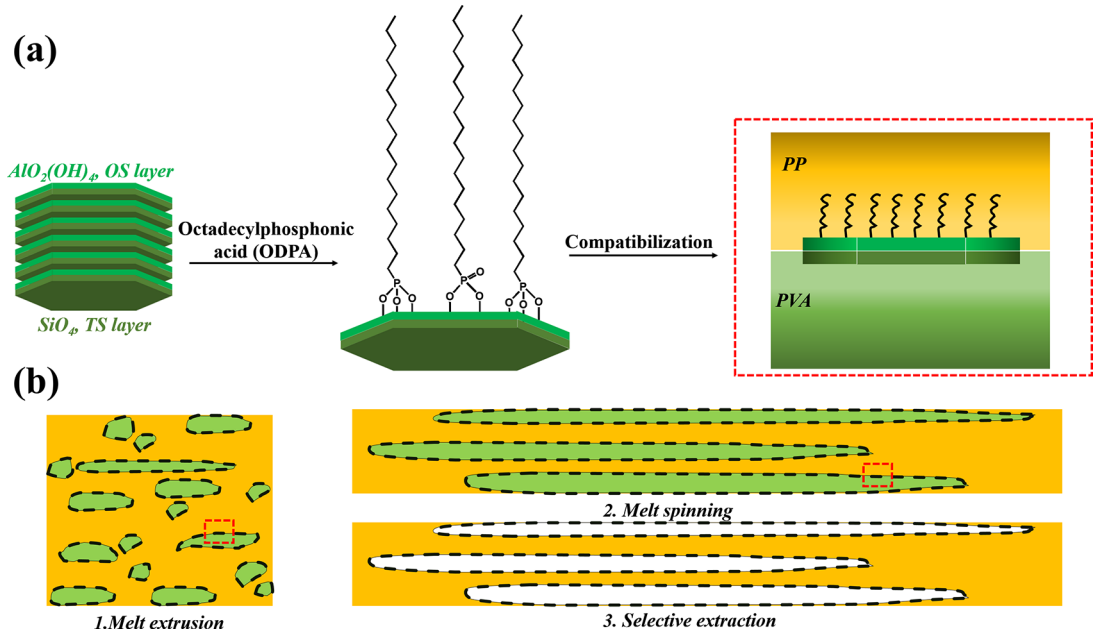

Figure 1. Schematic representation of (a) the synthesis of Janus kaolinite particles; (b) the manufacturing process of surface-modified porous PP fibers.

the polymer blends. The blend without fillers (denoted as PP_{70}-PVA_{30}) was compounded by one-step extrusion.

2.2.2. PP–PVA–Kaolinite Ternary Multifilament Fibers. The corresponding multifilament fibers were prepared from the obtained extrudates, via the melt-spinning machine (Busschaert model Spinboy I, Deerlijk, Belgium). Before melt spinning, the related extrudates were dried at 80 °C overnight to get rid of the moisture. The dried extrudates were introduced through the hopper and plasticized by a single screw. The temperatures along the barrel were regulated from 180 to 215 °C. The rotating speed of the volumetric pump was adjusted at 15 rpm. Hence, the molten polymer blends could be forced through two dies of 40 circular channels (diameter Ø of 1.2 mm) at a constant rate. Continuously fabricated multifilament yarns (80 monofilaments) were cooled through the air, followed by the treatment of finishing oil. Afterward, the multifilament fibers were rolled up onto two heated rolls (70–80 °C). Two distinct rotational speeds 100 rpm of the first roll and 200 rpm of the second roll were applied to realize a draw for the fibers. The theoretical drawing ratio (DR) can be settled as 2. The final winding speed was adapted to the same as the second draw roll.

2.2.3. Selective Extraction Experiment. In order to obtain the microporous PP material, the selective extraction experiment was conducted to remove the sacrificial PVA phase. The fraction of PVA would be recorded as a reference for the PVA continuity within the polymers. Water is an excellent selective solvent for PVA and has no impact to PP matrix. First, the samples (extrudates and multifilament fibers) of roughly 4 g and filter papers (dried at 80 °C, overnight) were weighed separately. The tested samples were immersed into a water batch under constant magnetic stirring for 5 h to ensure the thorough extraction. The solution along with the samples was then immediately poured onto the filter paper supported by a glass funnel. The remaining samples were rinsed by water several times and were left overnight at 50 °C. The dried porous samples can be obtained, and meanwhile, the PVA accessibility can be worked out by eq 1. The values were calculated by at least 2 times, and statistical data were acquired.

$$\text{PVA accessibility degree}(\%) = \frac{W_i - (W_{r+f} - W_f)}{W_i \times \omega_{PVA}} \times 100 \quad (1)$$

where W_i represents the initial weight of the dried samples, W_{r+f} indicates the total weight of samples jointed with the filter papers after the selective extraction experiment and drying, W_f represents the weight of the dried filter papers prior to use, and ω_{PVA} refers to the mass fraction of PVA within the polymer blends.

The synthesis of Janus kaolinite particles and the manufacturing process of surface-modified porous PP fibers are schematically represented in Figure 1.

2.3. Characterization. *2.3.1. Thermogravimetric Analysis (TGA).* The thermal stability of the fillers was tested by thermal gravimetric analyzer (Mettler Toledo). In order to get rid of the physisorbed water, an isothermal step with a temperature of 110 °C lasted for 10 min prior to conducting the analysis. Afterward, the tested samples were heated to 900 °C at a rate of 10 °C/min. TGA was carried out under two different atmospheres, nitrogen and air.

2.3.2. Scanning Electron Microscopy (SEM). The micromorphology observation of PP–PVA extrudates was conducted via a scanning electron microscope (FEI Quanta 200 ESEM). The sample was put in liquid nitrogen and broken by a hammer blow. The debris was placed on a pad of SEM and then metalized before analysis.

The morphology of the PP–PVA plate after rheometer measurement was also observed by an SEM apparatus (Inspect F, FEI Company). The dispersed PVA droplet sizes were determined by ImageJ analysis software (National Institutes of Health (NIH), Bethesda, MD, U.S.A.). More than 300 droplets were taken into account to ensure the accuracy. Afterward, Schwartz-Saltikov transformation[37] method was applied to correct the size distributions of the droplets. The method was operated by dividing the distribution into 7 linear

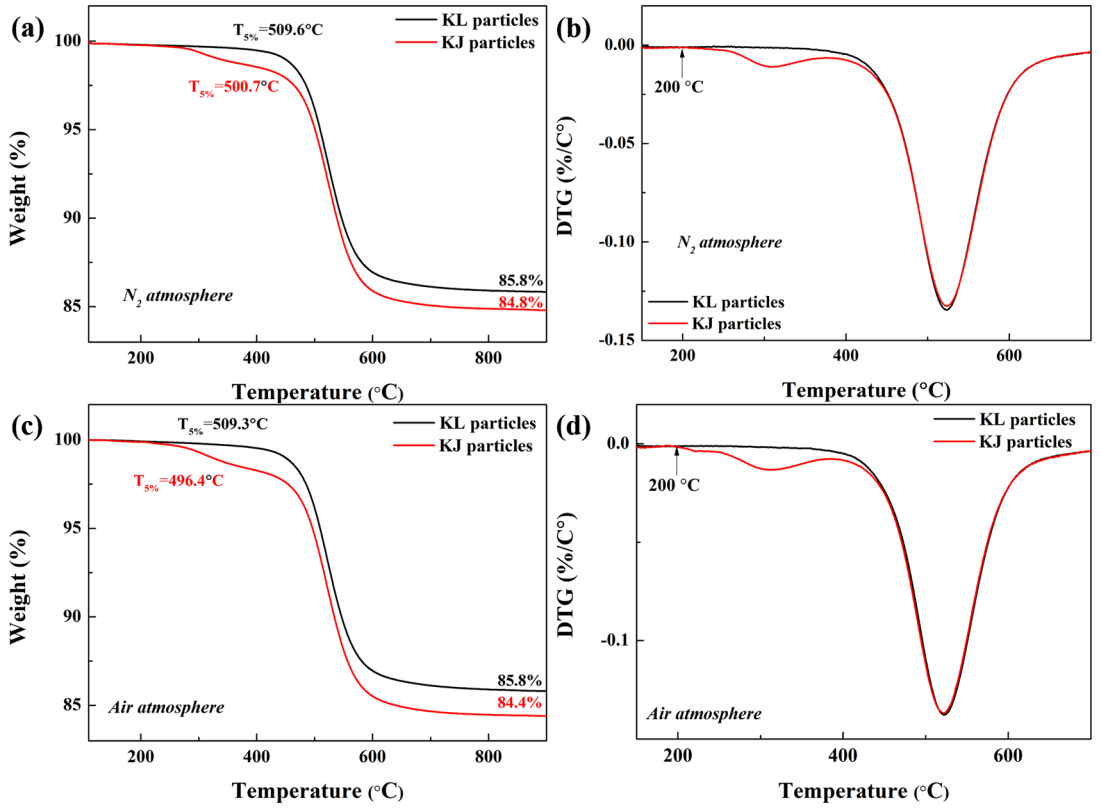

Figure 2. TG and DTG curves of KL and KJ particles in nitrogen and air atmosphere. (a) TG curves in a nitrogen atmosphere; (b) DTG curves in a nitrogen atmosphere; (c) TG curves in an air atmosphere; (d) DTG curves in an air atmosphere.

range groups, and the midpoint of each group represents the average value. The 3D particle distribution in volume can be transferred from the 2D particle distribution in area by applying the transformation coefficients.

2.3.3. Rheological Investigations. The rheological behaviors were surveyed on a rotational rheometer (AR 2000ex, TA Instruments, New Castle, DE, U.S.A.). The mode is selected as oscillatory characterization. The diameter of the parallel plate was 25 mm, and the gap distance was adjusted as 1500 μm. The frequency sweep was conducted from 100 to 0.01 rad/s, and all of the rheological measurements were operated at 190 °C.

2.3.4. Mechanical Properties. The single fibers were picked randomly from the multifilaments for mechanical measurement. The fibers were tested via a tensile machine (Zwick Roell Group, Ulm, Germany) equipped with a 10N load cell. The initial length of the gauge was set at 20 mm, and the measurement was conducted at the speed of 20 mm/min, All the measurements were carried out for 10 times, and the average values and the standard deviations were calculated. The measurements were operated under standard atmosphere (the temperature of 20 ± 2 °C, the relative humidity of 65 ± 5%).

2.3.5. DSC Measurement. Differential scanning calorimetry (DSC) measurements were carried out by using Mettler Toledo (Columbus, OH, U.S.A.) to analyze the melting behaviors of the tested fibers. The fibers were first to cut into powder and prepared for DSC measurement. The DSC analysis was conducted from 20 to 220 °C at a heating rate of 10 °C/min in a nitrogen atmosphere. In order to estimate the crystallinity degree (X_C), eq 2 was utilized:

$$X_c = \frac{\Delta H_f}{\Delta H_f^0} \times 100 \quad (2)$$

where ΔH_f is the heat of fusion of the tested powders (J/g) and ΔH_f^0 is the reference value that represents the heat of fusion for a perfect 100% crystalline polymer. For the case of PP, ΔH_f^0 can be regarded as 209 J/g.[38]

3. RESULTS AND DISCUSSION

3.1. Heat Resistance Properties of Kaolinites. The excellent thermal stability of the nanofillers at the processing temperature is an essential precondition for melt manufacturing. The initial decomposition temperature can give a valuable reference. For both KL and KJ particles, the initial decomposition temperature is around 500 °C at either nitrogen or air atmosphere (Figure 2a,c, respectively). The DTG curves are observable in Figure 2b,d. It is clearly shown that there is even no subtle decomposition below 200 °C. The melt extrusion and spinning were both conducted below 200 °C. The excellent thermal stability of KL and KJ particles ensures that it can be a stable modifier for the polymer blends. These analyses show also a higher weight loss for modified kaolinite which correspond to the degradation of the grafted ODPA. The weight loss when KJ is analyzed under air atmosphere (which corresponds to a total decomposition of the grafted organic part) gives a grafting rate of about 1.4 wt %.

3.2. Morphology of the Nanocomposites. The median grain size (d_{50}) of kaolinite can reach as large as 800 nm, which can provide enough pixels for detection by SEM Figure 3 shows the SEM images of the fractured samples of PP_{70}-PVA_{30} blends containing the different kaolinites. Combined with the BSE images of the SEM, the localization of the PVA can be

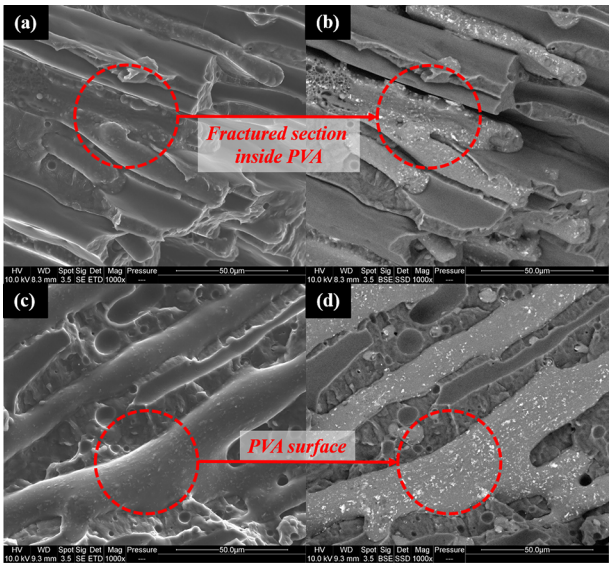

Figure 3. SEM images of PP_{70}-PVA_{30} blends with pristine and modified kaolinites (samples were cryo-fractured after treatment in liquid nitrogen). (a) PP_{70}-PVA_{30}-KL_5; (b) PP_{70}-PVA_{30}- KL_5 (BSE); (c) PP_{70}-PVA_{30}-KJ_5; (d) PP_{70}-PVA_{30}- KJ_5 (BSE).

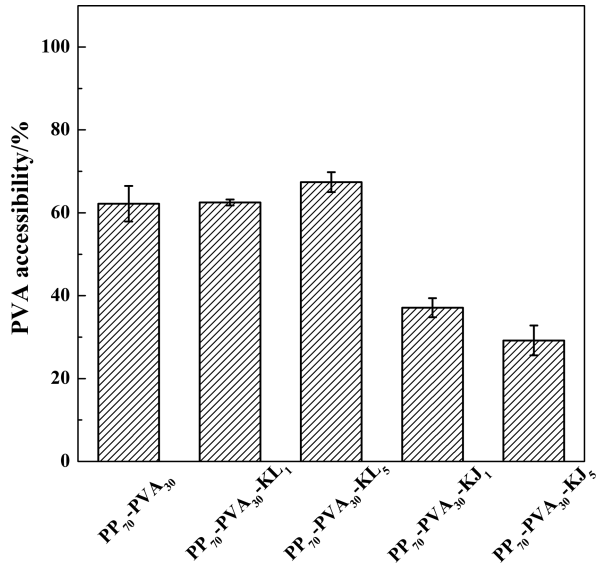

Figure 4. PVA accessibility degree of PP_{70}-PVA_{30} extrudates with pristine and modified kaolinites at 1 or 5 wt %.

easily distinguished. The light part stands for the PVA phase, and the dark part represents the PP phase. An additional EDS mapping has been conducted, and it has been found that the white dots are the kaolinite particles, with the detection of Si and Al element.

It can be observed that the shape of the PVA nodules is governed by continuous structure instead of the spherical structure, which is beneficial for the PVA connectivity in the matrix.[32] It can be distinguished that unmodified kaolinite KL particles are localized within the PVA phase, while Janus-modified kaolinite KJ particles are distributed at the biphasic interface. It can be concluded that the images show a location of a dominantly more substantial portion of kaolinite at the PP−PVA interface when it is modified.

The PVA accessibility degree of PP_{70}-PVA_{30} blends with two different kaolinites are illustrated in Figure 4. After the introduction of KL kaolinite nanoparticles, the PVA accessibility is not altered significantly and slightly enhanced by the addition of 5 wt % KL particles. As for the modified kaolinite, the addition leads to the dramatic decrease of PVA accessibility, which is related to the presence of the Janus kaolinite particles at the polymers interface. In our previous research, similar behaviors were investigated. It has been found that the PVA accessibility degrees are tightly relevant to the silica nanoparticles localization within the biphasic polymers, and the accessibility degree of the dispersed phase can even provide a route to predict the localization of the particles.[32] The filling of the unmodified kaolinite in the dispersed phase may slow down the effect of the destructive process, e.g., fibril breakup,[39] leading to the increment of PVA accessibility. As for the interface-located kaolinite, the effecting function is changed into steric hindrance or surfactants,[40] to prevent the coalescence of PVA phase.

In order to investigate the effect of kaolinite upon the size distribution of PVA nodules of the PP−PVA composites, SEM images of the cross-section of the plates after rheological tests are shown in Figure 5. The volume average diameter of PVA nodules within PP_{70}-PVA_{30} is 73.3 μm. The PVA nodules perform bimodal distribution, resulting from the annealing of initial spherical and elongated PVA nodules.[24] The initial elongated nodules were relaxed into the spherical PVA nodules with a high diameter value during the rheology test. After a long relaxation time, the deformed droplets evolve to recover the original spherical shapes.[41] The characteristic relaxation time of a slightly deformed droplet can be depicted by a concluded formula from Ultracki et al.[42,43]

$$\tau_d = \frac{(2p+3)(19p+16)\eta_m}{40(p+1)}\frac{R_0}{\sigma} \quad (3)$$

where p is viscosity ratio of dispersed phase to matrix phase, η_m represents the viscosity of the matrix, R_0 represents the radius of a droplet, and σ is the interfacial tension of the blends.

Equation 3 indicates that the retraction dynamics depends largely on the viscosity ratio, the interfacial tension, and droplet radius at equilibrium.[41] From the SEM observation of the cross sections, the PVA nodules within the blend samples without fillers can be reverted to spherical shapes after the rheology tests, demonstrating a complete relaxation. However, for the KL-containing PP−PVA blends, it cannot be completed changed into spherical shapes and keeps spheroidicity instead. Combined with the localization of KL inside PVA phase, it can be concluded that the increment of the relaxation time is due to the enhancement of the viscosity. What's more, there is also an increment of the size of the PVA nodules with the diameter of 126.1 μm and a dominant fraction of PVA nodules over 170 μm, which also needs a longer relaxation time, based on eq 3. It is worth noting that for the PP_{70}-PVA_{30}-KL_5 sample, the distribution of PVA nodules is too diverse; thus, the Schwartz-Saltikov transformation cannot be carried out due to the difficulty in statistics. Nevertheless, it can be clearly concluded that the PVA size is further increased with a higher amount of KL.

In contrast, it can be observed that the addition of modified kaolinite KJ leads to the refinement of PVA nodules. When 1 wt % of KJ particles are incorporated, the average diameter of PVA nodules is shifted to a lower value of 51.2 μm and a wide peak appears under 80 μm representing the majority volume fraction. It has been found that the PVA accessibility of KJ-

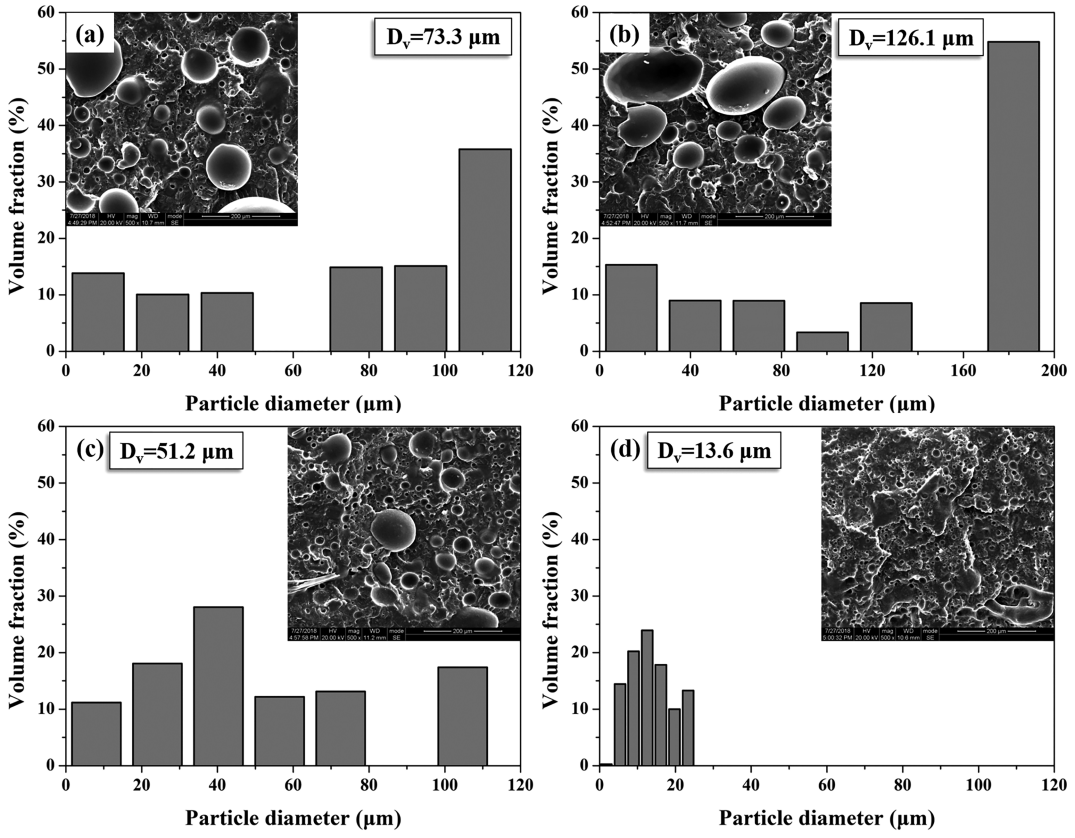

Figure 5. Particle diameter distribution and the SEM images of the PVA nodules inside PP matrix after the rheometer measurement (a) PP_{70}-PVA_{30}, (b) PP_{70}-PVA_{30}-KL_1, (c) PP_{70}-PVA_{30}-KJ_1, (d) PP_{70}-PVA_{30}-KJ_5.

containing extrudates is low, proving the PVA nodules have not formed a highly interconnected structure. In addition, it does not require a long relaxation time because of the small diameter of the PVA droplets. As a result, the PVA droplets also exhibit spherical shapes after the addition of Janus particles. After the addition of 5 wt % of KJ, the size of PVA nodules is significantly reduced and fused into one double peak under 30 μm. The volume average diameter is 13.6 μm for PP_{70}-PVA_{30}-KJ_5, presenting only 19% of the diameter of samples without nanoparticles. The refinement effect of KJ particles leads to a higher fraction of isolated PVA nodules in the extrudates, bringing about the drastic decrease of the PVA accessibility degree.

3.3. Rheological Characterization. The rheological results of PP_{70}-PVA_{30} blends with different kaolinites are displayed in Figure 6a,b. After the introduction of small amount of KL kaolinite particles, there is no distinct difference only leading to a slight enhancement of storage modulus and complex viscosity. For the unmodified kaolinite particles, when the adding amount is increased to 5 wt %, the enhancement effect is not elevated significantly. However, the storage modulus and complex viscosity of the PP_{70}-PVA_{30}-KJ_5 blend are significantly varied, reflected in the sudden and fierce increment in the low frequency, which proves that a gel-like (yield stress) behavior emerges. In order to demonstrate this phenomenon in depth, the pure polymer component was also tested for the rheological behaviors. PP exhibits a Newtonian plateau of complex viscosity at low shear rates, and instead PVA exhibits a distinctive behavior replaced by a sharp slope, resulting from the existence of dynamic hydrogen bonds between PVA molecules. However, it is worth noting that the storage modulus of the blends is higher than that of the PVA component, although PVA is only a minor phase inside the blends. What's more, the other filler-filling samples have no obvious gel-like behaviors. Related literature[24] revealed that this phenomenon is also attributed to the formation of a solid network of nanofillers (percolation) through the material. Generally speaking, the gel-like phenomenon of the blends originates from the joint effects of the biphasic percolation and hydrogen bonds inside PVA phase.

3.4. Melt Spinning of Nanocomposites. Values of the melt flow indices (MFI) for PP_{70}-PVA_{30} blends with pristine and modified kaolinites are listed in Figure 7. The MFI values related to the fluidity of the polymer composites are a very significant reference for the determination of melt spinning temperature, among which from 15 to 30 g/10 min the spinning process can be well-optimized. It can be found that the PP_{70}-PVA_{30} blends perform as the positive correlation compared with the pure components, with an MFI value of 30 ± 1.1 g/10 min (respectively 11.8 ± 0.6 g/10 min for PP and 19.3 ± 0.3 g/10 min for PVA). After the introduction of unmodified KL kaolinite particles, the MFI values are not altered obviously. However, it is not the same case with the incorporation of KJ Janus particles. The KJ particles can effectively decrease the fluidity of the blends (28.1 ± 1.0 g/10 min and 22.2 ± 0.3 g/10 min with 1 wt %/ 5 wt %, respectively) and so increase their viscosity. In the practical spinning, it was found that the temperature profiles had to be adjusted to a higher value to guarantee the success of melt spinning process.

PVA accessibility for PP_{70}-PVA_{30} fibers with KL and KJ is shown in Figure 8. Although the PVA accessibility of PP−PVA

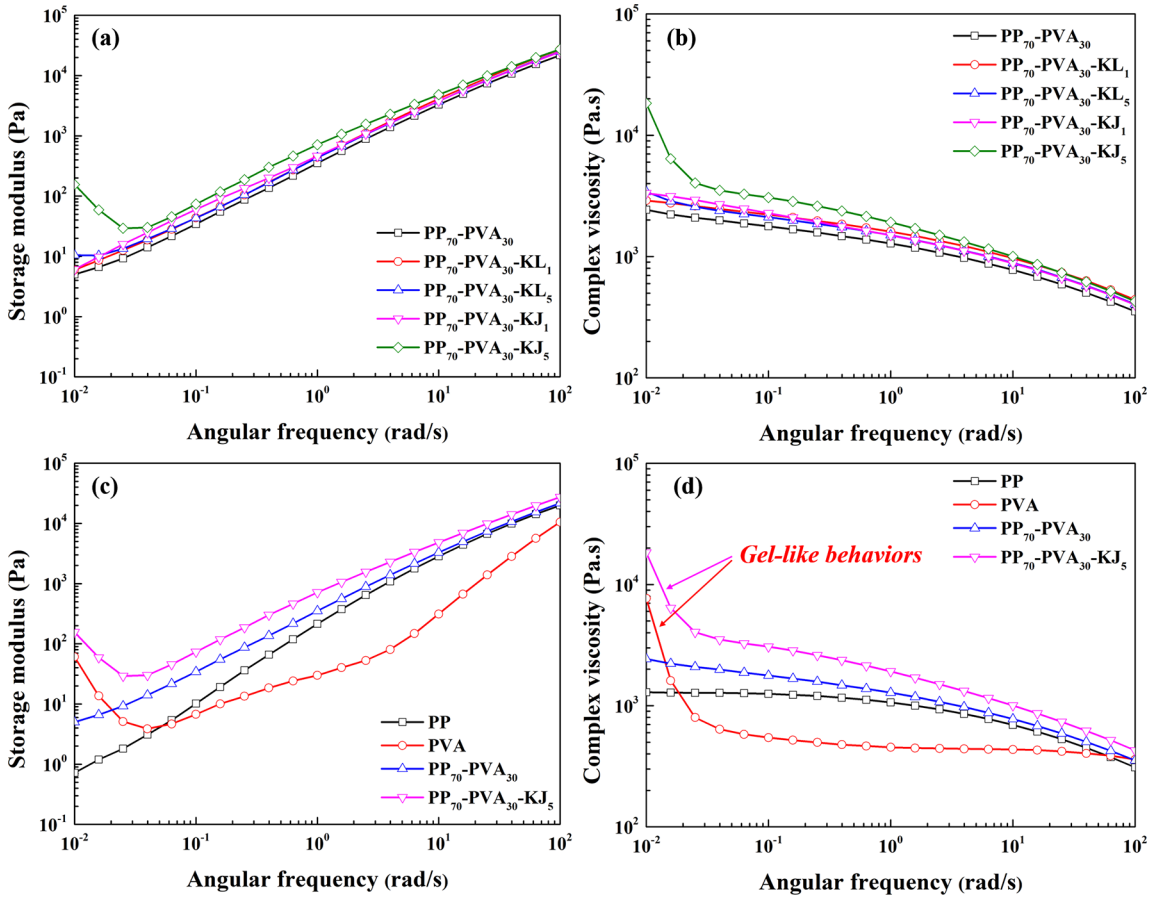

Figure 6. Rheological results of PP_{70}-PVA_{30} blends and pure components (a and b) storage moduli and complex viscosities of PP_{70}-PVA_{30} blends without/with kaolinite particles (c and d) storage moduli and complex viscosities of PP, PVA, PP_{70}-PVA_{30} blends without/with 5 wt % of KJ Janus particles.

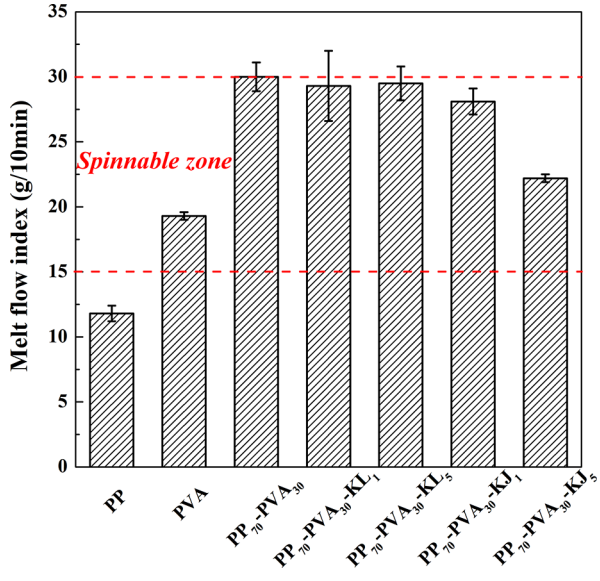

Figure 7. Melt flow index of PP_{70}-PVA_{30} blends with different kaolinites at 190 °C.

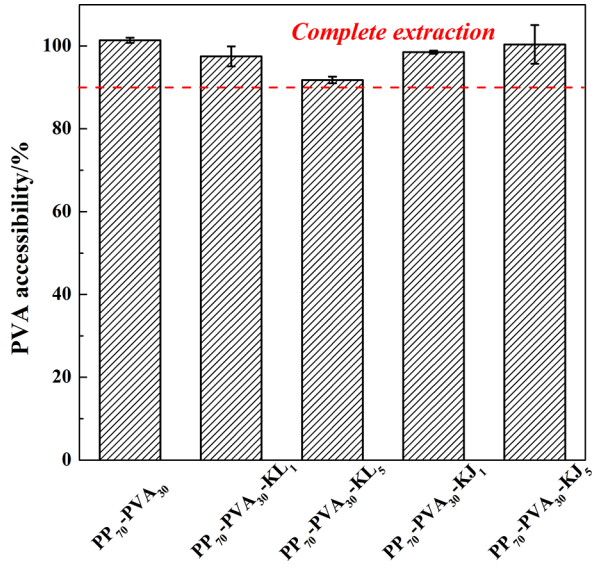

Figure 8. PVA accessibility of PP_{70}-PVA_{30} fibers with pristine and modified kaolinites.

blends is low (lower than 70%), especially for the blends with KJ Janus particles, the PVA accessibility degree can be elevated significantly due to the melt spinning process. It is inspiring that the PVA accessibility degree can always be over 90% for PP_{70}-PVA_{30} fibers even in the presence of kaolinite particles. All of the PVA phase can be removed after the selective extraction step, indicating that the PVA nodules are dominantly deformed and interconnected. A highly available PVA makes an excellent contribution to obtain a porous

Table 1. Mechanical Properties of PP_{70}-PVA_{30} Fibers Containing Kaolinite Particles and Neat PP Fibers

	before extraction			after extraction		
fibers	Young's modulus (MPa)	tenacity (cN/tex)	elongation at break (%)	Young's modulus (MPa)	tenacity (cN/tex)	elongation at break (%)
PP_{70}-PVA_{30}	1417 ± 136	11.4 ± 0.6	440 ± 39	1453 ± 316	12.2 ± 2.5	632 ± 41
PP_{70}-PVA_{30}-KL_1	1401 ± 96	10.2 ± 0.7	421 ± 40	1248 ± 195	11.2 ± 1.7	503 ± 54
PP_{70}-PVA_{30}-KL_5	1485 ± 248	9.5 ± 1.7	327 ± 74	1189 ± 294	8.4 ± 2.3	428 ± 76
PP_{70}-PVA_{30}-KJ_1	1657 ± 303	10.2 ± 1.0	408 ± 21	1413 ± 290	11.8 ± 2.0	604 ± 52
PP_{70}-PVA_{30}-KJ_5	2227 ± 370	12.2 ± 1.6	299 ± 82	1447 ± 395	11.7 ± 3.4	488 ± 80
PP	2174 ± 238	17.9 ± 2.2	516 ± 66			

material, endowed the multifilament yarns a high extraction efficiency toward the sacrificial phase.

In order to investigate the influence of kaolinite particles upon the mechanical properties of the multifilament yarns, tensile tests were conducted, and the related data are illustrated in Table 1. Moreover, the stress–strain curves are also displayed in Figure 9. The biphasic PP_{70}-PVA_{30} fibers exhibit good mechanical properties, with the Young's modulus of 1417 ± 136 MPa, tenacity of 11.4 ± 0.6 cN/tex, and elongation at break of 440 ± 39%. With the treatment of selective extraction, the Young's modulus and tenacity keep unchanged, with a significant increment of elongation at break to 632 ± 41%. The related stress–strain curves are displayed in Figure 9a. The shape of the curve for PP is similar to that of selectively extracted PP_{70}-PVA_{30}-Ex fibers, attributed to the component PP.

Figure 9b,c illustrates the stress–strain curves of the filaments without/with kaolinite particles and before and after selective extraction. After the introduction of KL particles, the mechanical properties are gradually weakened. The tenacity and breaking elongation are decreased, and Young's modulus is kept stable. After the introduction of 1 wt % of KJ particles into the blends, the tenacity and breaking elongation is decreased slightly and value of the Young's modulus is slightly increased. However, if 5 wt % of KJ is introduced, the Young's modulus is increased fiercely from 1417 ± 136 MPa for unfilled blends toward 2227 ± 370 MPa, with a sharp 57% increment. Meanwhile, its tenacity is slightly enhanced with a decrease of elongation at break. It proves that the introduction of the Janus particles significantly enhances the Young's modulus of the fibers, with a strengthening of the interface due to the particular localization of the kaolinite particles. The decrease in the breaking elongation also gives the evidence of the interfacial localization of the fillers. So Janus-modified particles can also be utilized in melt spinning technology fields, to offer a remedy and enhancement strategy for the weakening effect in mechanical properties of melt-spun fibers.

Meanwhile, after selective extraction, the breaking elongation is increased due to the removal of PVA. The tenacity has no significant change after the extraction. The Young's modulus is decreased at a different degree, and that of PP_{70}-PVA_{30}-KJ_5 is recovered near that of the filaments without fillers. It hints that the great mechanical contribution of the filaments with Janus particles mainly originates from PVA phase.

Melting points of PP and PVA are very close, which complicates the analysis of their crystallization degree. However, it is still of great interest to dig the related information on the PP porous fibers obtained after PVA extraction. Therefore, the DSC spectra of PP and PP_{70}-PVA_{30}-Exfibers (after selective extraction) are shown in Figure 10a,

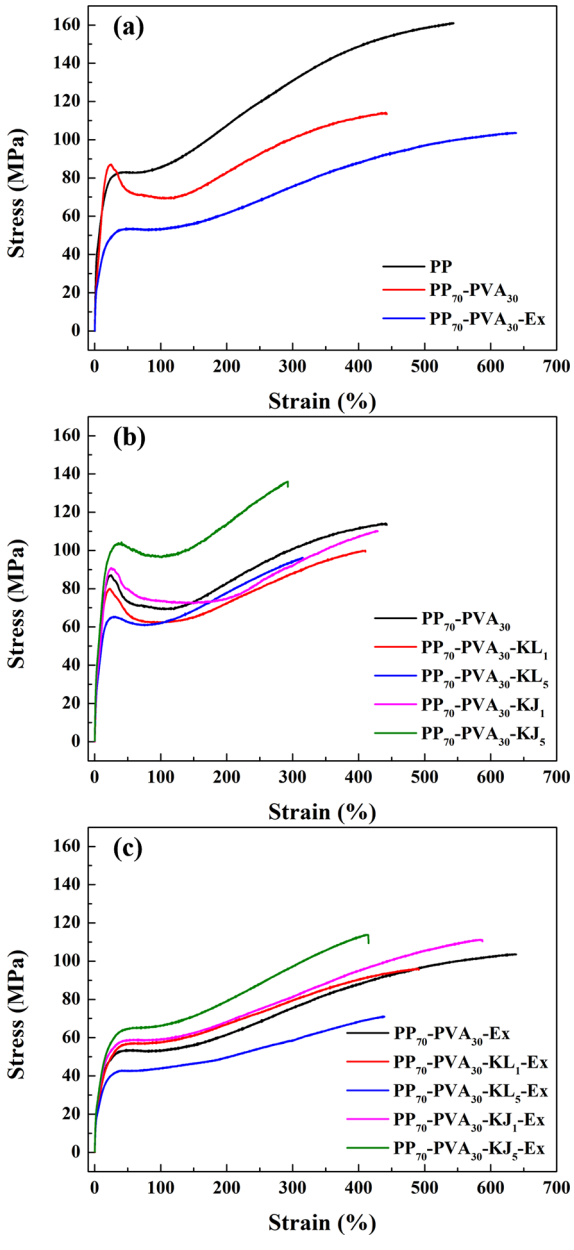

Figure 9. Stress–strain curves of PP_{70}-PVA_{30} fibers with pristine and modified kaolinite particles (a) before extraction; (b) after extraction; (c) neat PP fibers.

with data details in Table 2. Figure 10a shows that there is one peak around 166.5 °C for neat PP fibers. For PP_{70}-PVA_{30}-Ex fibers, the shape of the DSC spectra is similar to the adjacent melting point of 166.3 °C, while the crystallinity degree is decreased. It is one of the reasons that the mechanical

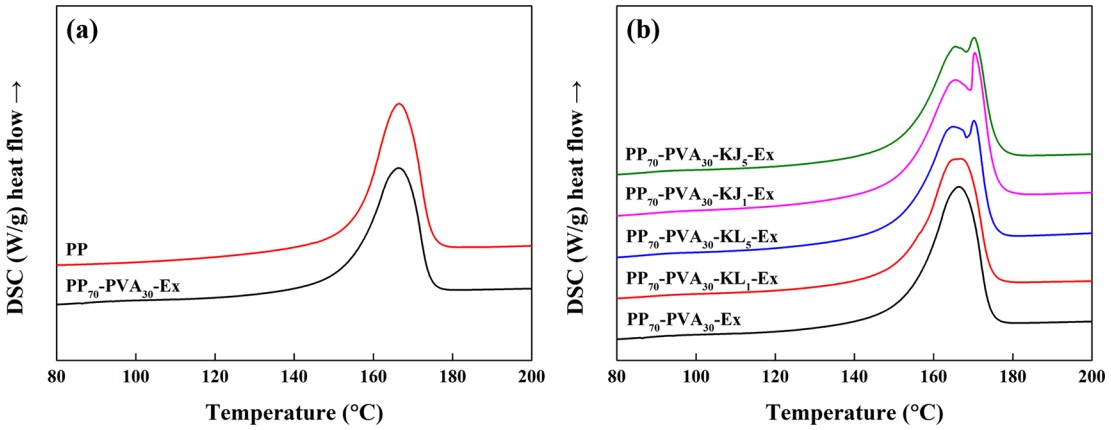

Figure 10. DSC spectra of (a) neat PP and PP_{70}-PVA_{30}-Ex and (b) PP_{70}-PVA_{30} without/with kaolinite particles after selective extraction.

Table 2. Thermal Properties of Neat PP and PP_{70}-PVA_{30} Fibers after Extraction

	enthalpy (J/g)	X_c (%)	T_{peak1} (°C)	T_{peak2} (°C)
PP	83.34	39.9	166.5	
PP_{70}-PVA_{30}-Ex	75.60	36.2	166.3	
PP_{70}-PVA_{30}-KL_1-Ex	72.77	34.8	166.8	
PP_{70}-PVA_{30}-KL_5-Ex	71.69	34.3	164.9	170.2
PP_{70}-PVA_{30}-KJ_1-Ex	80.26	38.4	165.5	170.4
PP_{70}-PVA_{30}-KJ_5-Ex	72.67	34.8	165.5	170.3

properties of PP_{70}-PVA_{30}-Ex fibers are weaker. It is also due to the generated porous structures forming tremendous stress concentration points. To investigate the influence of kaolinite particles to the crystallization of PP porous fibers, the DSC spectra of the composite fibers after extraction are shown in Figure 10b with details in Table 2 as well. The PP_{70}-PVA_{30}-Ex fibers show a single melting peak during heating, and the crystallization degree is not altered obviously after the addition of the clay. However, fibers obtained using kaolinite exhibit two endothermic maxima instead of a single peak. Compared with unmodified kaolinite, the impact of Janus particles to the DSC peak splitting is more significant. The peak splitting is associated with a degree of perfection of the crystals, of which the high-temperature endotherm is caused by the recrystallization due to more thermal energy.[44,45] It indicates that the perfection of the crystals is enhanced by the addition of the kaolinite particles, especially the Janus-modified ones.

4. CONCLUSION

We originally introduce Janus particles into melt spinning systems, with hybrid kaolinite as an example. The particles localize at the PP−PVA interface and significantly enhance the polymer compatibility. The melt-spun yarns from PP_{70}-PVA_{30} are mechanically improved, of which the Young's modulus is significantly increased. Meanwhile, the Janus modified kaolinite influences the morphology of the extrudates as well, reflected in the differentiated PVA accessibility. It also has obvious impact upon the rheological behavior. Indeed, rheological characterizations show a gel-like behavior for 5 wt % of KJ, originating from the PVA and from a percolation effect due to the interfacial localization of the Janus particles. The KJ-containing samples also exhibit lower melt flow indices. Furthermore, the PP crystallization rate decreases with the addition of the kaolinite particles even if the perfection of the crystals is improved.

AUTHOR INFORMATION

Corresponding Author

*E-mail: xiang.yan@ensait.fr. Tel.: + 33(0)3.20.25.86.90.

ORCID

Xiang Yan: 0000-0002-7985-4249

Notes

The authors declare no competing financial interest.

REFERENCES

(1) Panapitiya, N. P.; Wijenayake, S. N.; Nguyen, D. D.; Huang, Y.; Musselman, I. H.; Balkus, K. J., Jr; Ferraris, J. P. Gas Separation Membranes Derived from High-Performance Immiscible Polymer Blends Compatibilized with Small Molecules. *ACS Appl. Mater. Interfaces* **2015**, *7* (33), 18618−27.

(2) Oyama, H. T.; Nakayama, R.; Takase, K.; Furuta, M. Drastic improvement in thermal stability of polymer alloys by formation of daughter micelles at the reactive interface. *Polymer* **2018**, *137*, 107−11.

(3) de Luna, M. S.; Filippone, G. Effects of nanoparticles on the morphology of immiscible polymer blends - Challenges and opportunities. *Eur. Polym. J.* **2016**, *79*, 198−218.

(4) Bahrami, R.; Löbling, T. I.; Schmalz, H.; Müller, A. H.; Altstädt, V. Synergistic effects of Janus particles and triblock terpolymers on toughness of immiscible polymer blends. *Polymer* **2017**, *109*, 229−37.

(5) Brown, H. R.; Char, K.; Deline, V. R.; Green, P. F. Effects of a diblock copolymer on adhesion between immiscible polymers. 1. Polystyrene (PS)-PMMA copolymer between PS and PMMA. *Macromolecules* **1993**, *26* (16), 4155−63.

(6) Fortelný, I.; Juza, J. Analysis of the effect of block copolymers on interfacial tension in immiscible polymer blends. *Polymer* **2018**, *150*, 380−90.

(7) Huang, S.; Bai, L.; Trifkovic, M.; Cheng, X.; Macosko, C. W. Controlling the Morphology of Immiscible Cocontinuous Polymer Blends via Silica Nanoparticles Jammed at the Interface. *Macromolecules* **2016**, *49* (10), 3911−8.

(8) Chen, J.; Cui, X.; Sui, K.; Zhu, Y.; Jiang, W. Balance the electrical properties and mechanical properties of carbon black filled immiscible polymer blends with a double percolation structure. *Compos. Sci. Technol.* **2017**, *140*, 99−105.

(9) Kwon, T.; Kim, T.; Ali, F. B.; Kang, D. J.; Yoo, M.; Bang, J.; Lee, W.; Kim, B. J. Size-Controlled Polymer-Coated Nanoparticles as Efficient Compatibilizers for Polymer Blends. *Macromolecules* **2011**, *44* (24), 9852−62.

(10) Kodal, M. Polypropylene/polyamide 6/POSS ternary nanocomposites: Effects of POSS nanoparticles on the compatibility. *Polymer* **2016**, *105*, 43−50.

(11) Mederic, P.; Fneich, F.; Ville, J.; Aubry, T. Migration of clay and its role in droplet morphology establishment during melt mixing

of clay polyethylene/polyamide nanocomposites. *Appl. Clay Sci.* **2018**, *165*, 257−63.
(12) Tong, J.; Huang, H. X.; Wu, M. Promoting compatibilization effect of graphene oxide on immiscible PS/PVDF blend via water-assisted mixing extrusion. *Compos. Sci. Technol.* **2017**, *149*, 286−93.
(13) Chen, J.; Cui, X.; Zhu, Y.; Jiang, W.; Sui, K. Design of superior conductive polymer composite with precisely controlling carbon nanotubes at the interface of a co-continuous polymer blend via a balance of π-π interactions and dipole-dipole interactions. *Carbon* **2017**, *114*, 441−8.
(14) Wang, H.; Fu, Z.; Zhao, X.; Li, Y.; Li, J. Reactive Nanoparticles Compatibilized Immiscible Polymer Blends: Synthesis of Reactive SiO2 with Long Poly(methyl methacrylate) Chains and the in Situ Formation of Janus SiO2 Nanoparticles Anchored Exclusively at the Interface. *ACS Appl. Mater. Interfaces* **2017**, *9* (16), 14358−70.
(15) Pan, Y.; Liu, X.; Hao, X.; Starý, Z.; Schubert, D. W. Enhancing the electrical conductivity of carbon black-filled immiscible polymer blends by tuning the morphology. *Eur. Polym. J.* **2016**, *78*, 106−15.
(16) Huang, J.; Zhu, Y.; Xu, L.; Chen, J.; Jiang, W.; Nie, X. Massive enhancement in the thermal conductivity of polymer composites by trapping graphene at the interface of a polymer blend. *Compos. Sci. Technol.* **2016**, *129*, 160−5.
(17) Mural, P. K. S.; Banerjee, A.; Rana, M. S.; Shukla, A.; Padmanabhan, B.; Bhadra, S.; Madras, G.; Bose, S. Polyolefin based antibacterial membranes derived from PE/PEO blends compatibilized with amine terminated graphene oxide and maleated PE. *J. Mater. Chem. A* **2014**, *2* (41), 17635−48.
(18) Fenouillot, F.; Cassagnau, P.; Majesté, J. C. Uneven distribution of nanoparticles in immiscible fluids: Morphology development in polymer blends. *Polymer* **2009**, *50* (6), 1333−50.
(19) Yang, Q.; Loos, K. Janus nanoparticles inside polymeric materials: interfacial arrangement toward functional hybrid materials. *Polym. Chem.* **2017**, *8* (4), 641−54.
(20) Walther, A.; Matussek, K.; Muller, A. H. Engineering Nanostructured Polymer Blends with Controlled Nanoparticle Location using Janus Particles. *ACS Nano* **2008**, *2* (6), 1167−78.
(21) Bryson, K. C.; Löbling, T. I.; Müller, A. H.; Russell, T. P.; Hayward, R. C. Using Janus Nanoparticles To Trap Polymer Blend Morphologies during Solvent-Evaporation-Induced Demixing. *Macromolecules* **2015**, *48* (12), 4220−7.
(22) Bahrami, R.; Löbling, T. I.; Gröschel, A. H.; Schmalz, H.; Müller, A. H.; Altstädt, V. The Impact of Janus Nanoparticles on the Compatibilization of Immiscible Polymer Blends under Technologically Relevant Conditions. *ACS Nano* **2014**, *8* (10), 10048−56.
(23) Wang, H.; Dong, W.; Li, Y. Compatibilization of Immiscible Polymer Blends Using in Situ Formed Janus Nanomicelles by Reactive Blending. *ACS Macro Lett.* **2015**, *4* (12), 1398−403.
(24) Parpaite, T.; Otazaghine, B.; Caro, A. S.; Taguet, A.; Sonnier, R.; Lopez-Cuesta, J. M. Janus hybrid silica/polymer nanoparticles as effective compatibilizing agents for polystyrene/polyamide-6 melted blends. *Polymer* **2016**, *90*, 34−44.
(25) Xu, W.; Chen, J.; Chen, S.; Chen, Q.; Lin, J.; Liu, H. Study on the Compatibilizing Effect of Janus Particles on Liquid Isoprene Rubber/Epoxy Resin Composite Materials. *Ind. Eng. Chem. Res.* **2017**, *56* (47), 14060−8.
(26) Nie, H.; Liang, X.; He, A. Enthalpy-Enhanced Janus Nanosheets for Trapping Nonequilibrium Morphology of Immiscible Polymer Blends. *Macromolecules* **2018**, *51* (7), 2615−20.
(27) Sahnoune, M.; Taguet, A.; Otazaghine, B.; Kaci, M.; Lopez-Cuesta, J. M. Inner surface modification of halloysite nanotubes and its influence on morphology and thermal properties of polystyrene/polyamide-11 blends. *Polym. Int.* **2017**, *66* (2), 300−12.
(28) Sato, H.; Ono, K.; Johnston, C. T.; Yamagishi, A. First-principle study of polytype structures of 1:1 dioctahedral phyllosilicates. *Am. Mineral.* **2004**, *89* (11−12), 1581−5.
(29) Weiss, S.; Hirsemann, D.; Biersack, B.; Ziadeh, M.; Müller, A. H.; Breu, J. Hybrid Janus particles based on polymer-modified kaolinite. *Polymer* **2013**, *54* (4), 1388−96.
(30) Zhang, X.; Jin, G.; Ma, W.; Meng, L.; Yin, H.; Zhu, Z.; Dong, Z.; Wang, R. Fabrication and properties of poly(l-lactide) nanofibers via blend sea-island melt spinning. *J. Appl. Polym. Sci.* **2015**, *132*, 41228 DOI: 10.1002/app.41228.
(31) Huang, W.; Huang, X.; Wang, P.; Chen, P. Poly(glycolic acid) Nanofibers via Sea-Island Melt-Spinning. *Macromol. Mater. Eng.* **2018**, *303* (12), 1800425.
(32) Yan, X.; Cayla, A.; Devaux, E.; Salaün, F. Microstructure Evolution of Immiscible PP-PVA Blends Tuned by Polymer Ratio and Silica Nanoparticles. *Polymers* **2018**, *10* (9), 1031.
(33) Fakirov, S.; Bhattacharyya, D.; Panamoottil, S. M. Converting of Bulk Polymers Into Nanosized Materials With Controlled Nanomorphology. *Int. J. Polym. Mater.* **2014**, *63* (15), 777−93.
(34) Soltani, I.; Macosko, C. W. Influence of rheology and surface properties on morphology of nanofibers derived from islands-in-the-sea meltblown nonwovens. *Polymer* **2018**, *145*, 21−30.
(35) Rezanova, N.; Budash, Y.; Plavan, V.; Ishchenko, O.; Bulakh, V. Morphology and rheology of nanofilled PP/PVA blends. *Mater. Plast.* **2017**, *54*, 735−9.
(36) Gao, W.; Dickinson, L.; Grozinger, C.; Morin, F. G.; Reven, L. Self-Assembled Monolayers of Alkylphosphonic Acids on Metal Oxides. *Langmuir* **1996**, *12* (26), 6429−35.
(37) Saltikov, S. A. The Determination of the Size Distribution of Particles in an Opaque Material from a Measurement of the Size Distribution of Their Sections. *Stereology* **1967**, 163−73.
(38) Brandrup, J.; Immergut, E. H. *Polymer Handbook*, 3rd ed.; Wiley Interscience: New York, 1989.
(39) Steinmann, S.; Gronski, W.; Friedrich, C. Influence of selective filling on rheological properties and phase inversion of two-phase polymer blends. *Polymer* **2002**, *43* (16), 4467−77.
(40) Zhang, M.; Huang, Y.; Kong, M.; Zhu, H.; Chen, G.; Yang, Q. Morphology and rheology of poly(l-lactide)/polystyrene blends filled with silica nanoparticles. *J. Mater. Sci.* **2012**, *47* (3), 1339−47.
(41) Wu, D.; Yuan, L.; Laredo, E.; Zhang, M.; Zhou, W. Interfacial Properties, Viscoelasticity, and Thermal Behaviors of Poly(butylene succinate)/Polylactide Blend. *Ind. Eng. Chem. Res.* **2012**, *51* (5), 2290−8.
(42) Luciani, A.; Champagne, M. F.; Utracki, L. A. Interfacial tension coefficient from the retraction of ellipsoidal drops. *J. Polym. Sci., Part B: Polym. Phys.* **1997**, *35* (9), 1393−403.
(43) Kong, M.; Huang, Y.; Chen, G.; Yang, Q.; Li, G. Retarded relaxation and breakup of deformed PA6 droplets filled with nanosilica in PS matrix during annealing. *Polymer* **2011**, *52* (22), 5231−6.
(44) Cho, D.; Zhou, H.; Cho, Y.; Audus, D.; Joo, Y. L. Structural properties and superhydrophobicity of electrospun polypropylene fibers from solution and melt. *Polymer* **2010**, *51* (25), 6005−12.
(45) Torre, J.; Cortazar, M.; Gomez, M.; Ellis, G.; Marco, C. Melting behavior in blends of isotactic polypropylene and a liquid crystalline polymer. *J. Polym. Sci., Part B: Polym. Phys.* **2004**, *42* (10), 1949−59.